

Quantum entanglement and chaos in kicked two-component Bose-Einstein condensates

Q. Xie and W. Hai^a

Department of physics, Hunan Normal University, Changsha 410081, P.R. China

Received 4 January 2005 / Received in final form 31 January 2005

Published online 3 May 2005 – © EDP Sciences, Società Italiana di Fisica, Springer-Verlag 2005

Abstract. We study two-component Bose-Einstein condensates that behave collectively as a spin system obeying the dynamics of a quantum kicked top. Depending on the nonlinear interaction between atoms in the classical limit, the kicked top exhibits both regular and chaotic dynamical behavior. The quantum entanglement is physically meaningful if the system is viewed as a bipartite system, where the subsystem is any one of the two modes. The dynamics of the entanglement between the two modes in this classical chaotic system has been investigated. The chaos leads to rapid rise and saturation of the quantum entanglement. Furthermore, the saturated values of the entanglement fall short of its maximum. The mean entanglement has been used to clearly display the close relation between quantum entanglement and underlying chaos.

PACS. 03.75.Gg Entanglement and decoherence in Bose-Einstein condensates – 05.45.Mt Quantum chaos; semiclassical methods – 03.75.Kk Dynamic properties of condensates; collective and hydrodynamic excitations, superfluid flow – 05.30.Jp Boson systems

1 Introduction

In recent years, quantum entanglement (referred to hereafter as entanglement) has been regarded as a physical resource which can be exploited to perform many useful tasks in quantum information processing [1–5]. Studies of the entanglement characteristics of various interacting many-body systems have also given exciting new insight into the fundamental aspects of quantum physics. Latterly, a new emphasis has emerged that entanglement can be related to the properties of a many-body system. Since entanglement is responsible for the appearance of long-range correlations, it has been demonstrated that it plays a crucial role in the study of quantum phase transitions (QPTs) [6–10]. There have also been recent attempts to relate localization and bifurcation to entanglement [11–15].

However, much more attention has been paid to the connection between entanglement and classical chaos, because of the challenges in identifying quantum signature in classically chaotic systems [16–19]. Such a connection has been previously examined with the help of several different models, including an N -atom Jaynes-Cummings model, kicked top, coupled kicked top and Dicke model, as well as the XY model. For example, it was found for the N -atom Jaynes-Cummings model that the entanglement rate, quantitatively expressed in terms of the reduced density linear entropy between the atom system

and the radiation field, is considerably enhanced if the initial wave packet is prepared in a chaotic region [20, 21]. The work of Miller and Sarkar has shown that a similar property also exists in the weakly coupled tops, and the von Neumann entropy of the subsystem linearly depends on the sum of positive Lyapunov exponents of the corresponding classical system [22]. Along these lines, it was further found that the increment of the chaos strength does not enhance the production rate of the entanglement in the same system [23, 24]. Very recently, the mean entanglement over time has been used to identify the edge of chaos in the Dicke and top model [25, 26]. Although a complete theory for many-body entanglement is still lacking, most studies of the entanglement in a chaotic system have employed the bipartite entanglement for pure state and the pairwise entanglement of qubit pairs in a multi-qubit system. For bipartite entanglement, where the total system is divided into two subsystems, the entropies of a subsystem, for example, the von Neumann and linear entropies, are used to quantify the amount of entanglement the two subsystems have. Pairwise entanglement, on the other hand, considers the degree of entanglement of qubit pairs, where the concurrence is adopted as the measure of the entanglement. Recent results have supported the conclusion that chaos can cause the increase of the bipartite entanglement, but leads to reduction of the pairwise entanglement [11, 26, 27]. This means that the entanglement behavior associated with the chaotic parameter regions depends on the measure of the entanglement. Therefore, it will be very interesting to further understand these

^a e-mail: adcve@public.cs.hn.cn

properties of entanglement for other system with different entanglement measures. In particular, some authors have also employed the purity fidelity of a reduced density matrix for a composite quantum system as a different entanglement measure to find qualitatively different decay behaviors between the integrable and chaotic systems [28].

Recently produced two component Bose-Einstein condensates (BECs) provide us with a different system [29] to the above-mentioned ones, which are often viewed as a collection of N single qubit subsystems. Hines and co-workers claimed that the decomposition of the BECs system into subsystems consisting of individual bosons is not physically realizable due to the indistinguishability of the boson within the condensates [30], and the entanglement is only physically meaningful if the system is viewed as a bipartite, where the two subsystems are the two modes. In the present paper, we propose a scheme to realize the well-known nonlinear quantum top in two-component Bose-Einstein condensates (BECs). Although the relation between entanglement and classical chaos have been studied in detail for the quantum top in reference [26], the system under the previous consideration is regarded as a collection of N single qubit subsystems. Here we consider the two component BEC as two modes as in the electromagnetism field, and investigate the relation between the mode entanglement and classical chaos in the kicked two-component BEC system. In the two BEC system, some well-known results for the quantum top will express new physical meaning. For example, in the classical limit, an increase in the strength of interaction between atoms, which can be tuned by Feshbach resonance [31], can drive the system gradually from a mainly regular motion to a dominantly chaotic one. In the strong interaction limit, the system can be turned into a quantum kicked rotor in phase presentation. Therefore, the two component BEC system provides a good test ground for the study of quantum chaos. Here the von Neumann entropy of the subsystem is employed to measure the mode entanglement comparing to the linear entropy and concurrence used in reference [26]. Our results support the previous conclusion that the von Neumann entropy increases more rapidly for an initial state localized in the chaotic region than for one centered on a fixed point, but a closer classical-quantum correspondence may be demonstrated in terms of the mode entanglement. Different from the linear entropy used for distinguishable qubit systems in reference [26], the von Neumann entropy can here have nonzero initial values, whether the initial conditions are in the chaotic sea or not. Furthermore, the entropy for a fixed point or stable orbit displays a more clearly periodic modulation after a fast increase for a short time, which is an indicator of the underlying regular classical dynamics. If the initial states are in the chaotic region, the classical chaos leads the entropy to rise more rapidly and to arrive at a saturation of the quantum entanglement in a chaotic oscillatory manner rather than the oscillatory increase shown in reference [26]. In order to better understand the classical-quantum correspondence, the mean entanglement, which is defined to be averaged over time, is also applied to describe the distinct

changes at and near the boundary between the regular and chaotic motions.

This paper is organized as follows: in Section 2, we shall derive a two mode Hamiltonian describing the two-component BECs interacting with a classical near-resonant laser that is rapidly and periodically switched on and off in time to approximate a series of delta functions. It will be found that the system behaves collectively as a quasispin-1/2 obeying the dynamics of the quantum kicked top. In the investigation of the quantum and classical dynamics, we show that the system can be turned into a standard quantum rotor in the phase representation at a strong interaction limit. The validity of the two-mode approximation is also discussed in this section. In Section 3, we consider the evolution of the mode entanglement and establish the close correspondence between the quantum entanglement and classical chaos. Using the mean entanglement, we examine the edge of the quantum chaos. In Section 4, a simple discussion and a final conclusion are made.

2 The quantum kicked top in the two-component BECs

2.1 A scheme for realizing a quantum kicked top

We consider a zero-temperature two-component BEC system which consists of N atoms trapped in two different hyperfine states $|a\rangle$ and $|b\rangle$ coupled by a near-resonant Raman laser [29]. Within the formalism of the second quantization, the Hamiltonian of the system is of the form [32, 33]

$$\hat{H} = \hat{H}_a + \hat{H}_b + \hat{H}_{int} + \hat{H}_{ext}, \quad (1)$$

$$\hat{H}_i = \int d^3\vec{r} \Psi_i^\dagger(\vec{r}) \left[-\frac{\hbar^2}{2m} \nabla^2 + V_i(\vec{r}) + \frac{1}{2} U_{ii} \Psi_i^\dagger(\vec{r}) \Psi_i(\vec{r}) \right] \Psi_i(\vec{r}) \quad (i = a, b), \quad (2)$$

$$\hat{H}_{int} = U_{ab} \int d^3\vec{r} \Psi_a^\dagger(\vec{r}) \Psi_a(\vec{r}) \Psi_b^\dagger(\vec{r}) \Psi_b(\vec{r}), \quad (3)$$

$$\hat{H}_{ext} = \frac{1}{2} \int d^3\vec{r} \left[\Omega_R(t) \Psi_a^\dagger(\vec{r}) \Psi_b(\vec{r}) + \Omega_R^*(t) \Psi_b^\dagger(\vec{r}) \Psi_a(\vec{r}) \right]. \quad (4)$$

Here H_i expresses the non-coupling part of the Hamiltonian, H_{int} describes the collisions between the interspecies and H_{ext} denotes the coupling with the external field. Atoms of mass m are trapped in the potential $V_i(\vec{r})$, which can be regarded to be identical for different i . $U_{ij} = 4\pi\hbar^2 a_{ij}^{sc}/m$ ($i, j = a, b$) measure the interaction strengths between intra- and inter-component collisions, where a_{ii}^{sc} is s -wave scattering length of condensate i and a_{ab}^{sc} is that between condensates a and b . $\Psi_i(\vec{r})$ are bosonic field operators which destroy a particle at position \vec{r} in the hyperfine state $|i\rangle$, and satisfy the commutation relation $[\Psi_i(\vec{r}), \Psi_j^\dagger(\vec{r}')] = \delta_{ij} \delta(\vec{r} - \vec{r}')$. The effective Rabi frequency $\Omega_R(t)$ is assumed to be positive, real and position independent but periodically time dependent.

The Hamiltonian (1) can be reduced to a simple two mode Hamiltonian by an approximate expansion of the atomic field operator: $\Psi_a(\vec{r}) = \hat{a}\phi_a(\vec{r})$ and $\Psi_b(\vec{r}) = \hat{b}\phi_b(\vec{r})$, where \hat{a} and \hat{b} are particle annihilation operators obeying the relation $[i, j^\dagger] = \delta_{ij}$, $i, j = a, b$ with the spatial and normalized mode functions $\phi_a(\vec{r})$ and $\phi_b(\vec{r})$. Dropping the c -number terms, the Hamiltonian can be expressed in terms of $\hat{a}(\hat{a}^\dagger)$ and $\hat{b}(\hat{b}^\dagger)$ ($\hbar = 1$)

$$\hat{H} = \frac{u}{4}(\hat{a}^\dagger\hat{a} - \hat{b}^\dagger\hat{b})^2 + \frac{\Omega(t)}{2}(\hat{a}^\dagger\hat{b} + \hat{b}^\dagger\hat{a}), \quad (5)$$

where $u = (u_{aa} + u_{bb} - 2u_{ab})/2$ and

$$u_{ij} = U_{ij} \int d^3\vec{r} |\phi_i(\vec{r})|^2 |\phi_j(\vec{r})|^2, \\ \Omega(t) = \Omega_R(t) \int d^3\vec{r} \phi_a^*(\vec{r}) \phi_b(\vec{r}). \quad (6)$$

The two-mode Hamiltonian (5) is similar to these applied to consider the tunnelling dynamics and self-trapping between the double-well potential [34]. For the case of the Rabi frequency Ω_R time-independence, a simple and efficient method has been presented to solve the model for arbitrary (small or huge) total atom number N [37]. The constant u can be positive or negative depending on the mixture of different components in the real spinor BECs [38].

Rapidly and periodically switching the laser on and off with the time interval T , $\Omega_R(t)$ can be approximated by a train of Gaussian pulses [39]

$$\Omega_R(t) = \Omega_0 \sum_{n=0}^{\infty} \exp(-(t - nT)^2/\sigma^2), \quad (7)$$

which approaches a δ -function pulse in the limit $\sigma \rightarrow 0$,

$$\Omega_R(t) = \sqrt{\pi}\sigma\Omega_0 \sum_{n=0}^{\infty} \delta(t - nT) \quad (8)$$

with Ω_0 being proportional to the laser intensity.

In addition, we introduce the angular momentum operator \hat{J} in terms of the two boson modes

$$\hat{J}_x = \frac{1}{2}(\hat{a}^\dagger\hat{b} + \hat{b}^\dagger\hat{a}), \quad \hat{J}_y = \frac{i}{2}(\hat{b}^\dagger\hat{a} - \hat{a}^\dagger\hat{b}), \\ \hat{J}_z = \frac{1}{2}(\hat{a}^\dagger\hat{a} - \hat{b}^\dagger\hat{b}), \quad (9)$$

for which the Casimir invariant is $\hat{J}^2 = (\hat{N}/2)(\hat{N}/2 + 1)$, where $\hat{N} = \hat{a}^\dagger\hat{a} + \hat{b}^\dagger\hat{b}$ commutes with the Hamiltonian and is the total atom number of the system. Thus, the effective Hamiltonian (5) of the system can be reexpressed as

$$\hat{H} = u\hat{J}_z^2 + k\hat{J}_x \sum_{n=0}^{\infty} \delta(t - nT) \quad (10)$$

with $k = \sqrt{\pi}\sigma\Omega_0 \int d^3\vec{r} \phi_a^*(\vec{r}) \phi_b(\vec{r})$ referred to as the kicked strength. The Hamiltonian (10) describes a well-known

nonlinear quantum top model which exhibits chaos in the classical limit, and enjoys the privilege of a finite-dimensional Hilbert space due to the conservation of $\hat{J}^2 = (\hat{N}/2)(\hat{N}/2 + 1)$. Recently, Milburn has suggested a scheme to realize a similar nonlinear quantum top model on a linear ion trap [40]. Such a periodically kicked collective spin system can also be produced using ferromagnetic resonance at very high signal powers [41], which is now an attractive candidate to study classical and its quantum counterpart [42].

2.2 The quantum and classical dynamics

The quantum and classical dynamics of the kicked top have been studied in depth by some authors [16, 43]. Here we shall only introduce some important results. As an appropriate description, the Floquet operator transporting the state vector from immediately after one kick to immediately after the next reads

$$\hat{F} = e^{-ikT\hat{J}_x} e^{-iu\hat{J}_z^2}, \quad (11)$$

by which the quantum map is created. For the rest of the paper, we will focus our attention on the case $k = \pi/2$ and $T = 1$, such that the effective Hamiltonian (10) becomes

$$\hat{H} = \frac{\lambda}{N} \hat{J}_z^2 + \frac{\pi}{2} \hat{J}_x \sum_{n=0}^{\infty} \delta(t - n), \quad (12)$$

to simplify both quantum and classical dynamics. Here we have set $\lambda = Nu$.

It is natural to choose the simultaneous eigenstates of \hat{J}^2 and \hat{J}_z as a basis, which form $N + 1$ basis vectors defined by

$$\hat{J}^2|j, m\rangle = j(j+1)|j, m\rangle, \quad \hat{J}_z|j, m\rangle = m|j, m\rangle, \quad (13)$$

where

$$|j, m\rangle = \frac{(\hat{a}^\dagger)^{N/2+m} (\hat{b}^\dagger)^{N/2-m}}{\sqrt{(N/2+m)!(N/2-m)!}} |vac\rangle. \quad (14)$$

Here the values of m are taken from $-N/2$ to $N/2$ and $j = N/2$, and $|vac\rangle$ denotes the vacuum state. The matrix elements of \hat{F} in these states are simply given by

$$\langle j, m | \hat{F} | j, m' \rangle = \exp \left[-i \frac{\lambda}{N} m^2 + i \frac{\pi}{2} (m - m') \right] d_{mm'}^{(j)} \left(\frac{\pi}{2} \right), \quad (15)$$

in which $d_{mm'}^{(j)}(\beta)$ is the Wigner d function defined by

$$d_{mm'}^{(j)}(\beta) = \sum_l (-1)^{l-m'+m} \frac{\sqrt{(j+m')!(j-m')!(j+m)!(j-m)!}}{(j+m'-l)!l!(j-l-m)!(l-m'+m)!} \\ \times \cos^{(2j-2l+m'-m)} \left(\frac{\beta}{2} \right) \sin^{(2l-m'+m)} \left(\frac{\beta}{2} \right) \quad (16)$$

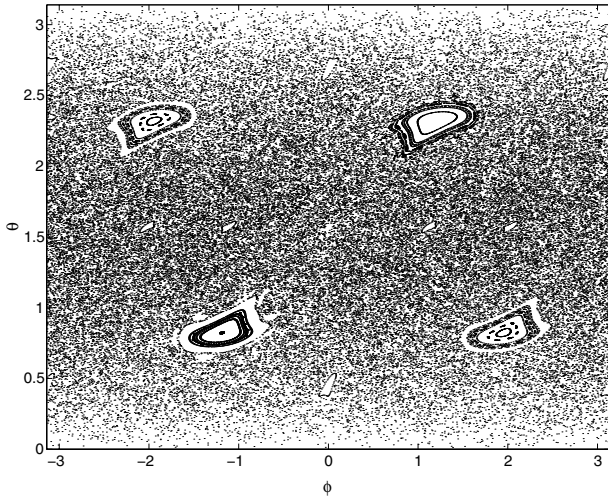


Fig. 1. Phase space plot for the classical kicked top with $\lambda = 3.5$. Three hundred trajectories are plotted, each for a duration of 300 kicks.

for arbitrary (either all integer or all half-integer) values of j, m, n' such that $|m| \leq j$ and $|m'| \leq j$. The summation over l runs from $\max(0, m + m')$ to $\min(j + m, j + m')$.

By approximating second order expectation values $\langle \hat{J}_i \hat{J}_j \rangle$ as a product of the first order expectation values $\langle \hat{J}_i \rangle$ and $\langle \hat{J}_j \rangle$, the corresponding classical dynamics is described by the three-dimensional map

$$\begin{aligned} X_{n+1} &= X_n \cos(\lambda Y_n) + Z_n \sin(\lambda Y_n), \\ Y_{n+1} &= X_n \sin(\lambda Y_n) - Z_n \cos(\lambda Y_n), \\ Z_{n+1} &= Y_n, \end{aligned} \quad (17)$$

where $X = \langle \hat{J}_x \rangle / j$, $Y = \langle \hat{J}_y \rangle / j$ and $Z = \langle \hat{J}_z \rangle / j$, and n denotes the kicked time. The variables X, Y and Z are related by $X^2 + Y^2 + Z^2 = 1$, and the restriction reduces the classical map to two dimensions, such that (X, Y, Z) can be reparameterized as $(X, Y, Z) = (\sin \theta \cos \phi, \sin \theta \sin \phi, -\cos \theta)$, where θ and ϕ are the polar and azimuthal angles, respectively. Generally, fixing $k = \pi/2$ the system is in regular motion for the parameter region $\lambda \leq 2.5$, whereas chaos prevails in the region $\lambda \geq 3$. In Figure 1, we give the classical phase space plot of a kicked top when the nonlinear parameter $\lambda = 3.5$, for which there are a mixture of regular and chaotic areas of significant size. Three areas will be of particular interest to us in the following. The first clearly reside in a stable island, which surrounds a fixed point $(\theta, \phi) = (2.32, 1.19)$ of the classical map given above. The second is in the chaotic sea and nowhere near a regular island. The third lies between the extremes of regular and chaotic behavior. As will be seen later, the dynamics of quantum entanglement in the quantum kicked top closely depends on this phase space structure of the classical kicked top.

2.3 A kicked rotor as a limiting case of the top

In classical dynamics, increasing λ more and more leads the system to strong chaos. We recall that $\lambda = Nu$ can

be regarded as a parameter measuring the strength of interaction between particles. Recently, the influence of the interaction between atoms on the dynamics in several chaotic BEC systems have been a subject of considerable interest [44–50]. We now proceed to show that in a strong interaction regime, the quantum kicked top can be turned into a quantum kicked rotor model. We use the eigenstates of the operator \hat{J}_z to construct the eigenstates of the relative phase between the two component condensates

$$|\phi\rangle = \frac{1}{\sqrt{2\pi}} \sum_{n=-N/2}^{N/2} e^{-in\phi} |j, n\rangle. \quad (18)$$

In the experiment, on one hand, the kick strength may be a very small value due to adjustable parameter σ and Ω_0 . On the other hand, the interaction can be tuned from $-\infty$ to ∞ by Feshbach resonance [31]. These facts may make the conditions $k \ll uN$ and $N \gg 1$ hold. In the phase representation, one can use the replacements $\hat{J}_z \rightarrow -i\partial_\phi$ and $\hat{J}_x \rightarrow (N/2) \cos \phi$ [32, 51], so that we can rewrite the Hamiltonian (10) as

$$\hat{H} = -u \frac{\partial^2}{\partial \phi^2} + kN/2 \cos \phi \sum_{n=0}^{\infty} \delta(t - nT) \quad (19)$$

which is similar to the standard QKR model [52]. Therefore, we can apply the phase model to study the many-body effects due to the parameter u describing the interaction.

2.4 Validity of the two-mode approximation

In making the calculation above, we have relied heavily on the two-mode approximation, essentially consisting in neglecting all modes except the condensate modes. At zero temperature, this amounts to ignoring the atoms which have left the condensate mode due to the two-body interactions. In order for this approximation to provide a reasonably accurate picture, we have also assumed that the parameters $u_{aa,bb,ab}$, u , Ω_0 and k are reasonably constants for the cases studied. However these parameters all depend on the self-consistently defined condensate modes of the system, which in turn depend on the particle numbers N_a and N_b . Thus the two-mode approximation will be most accurate when the dependence of the density profile on the particle number distribution is weak. The valid conditions of the two-mode approximation were demonstrated in [35, 36], which indicate that this approximation provides a reasonably accurate picture for the following conditions: (i) the weak many-body interactions, i.e., small number of condensed atoms. For the large condensates, the mode functions of condensates are altered due to the collisional interactions, and the two-mode approximation breaks down. As shown in [35], a simple estimate exhibits that this happens when the number of atoms $N a^{sc} \ll r_0$, where a^{sc} is a typical scattering length and r_0 is a measure of the trap size. If we consider a large

trap with the size $r_0 = 10 \mu\text{m}$ and the typical scattering length $a^{sc} = 5 \text{ nm}$, the two-mode approximation is applicable for $N \leq 2000$ in principle. (ii) The case in which $a_{aa}^{sc} \approx a_{bb}^{sc}$ and a_{ab}^{sc} is only slightly less than $a_{aa,bb}^{sc}$. There is exactly the experimental set-up used in reference [38], in which these selected hyperfine states $|F = 1, M_F = \pm 1\rangle$ of natrium approximately satisfy the above mentioned conditions. This is the case that we will consider here, and then the parameter u takes positive value in our following calculation. (iii) Weak coupling between two-component BECs. In this case, weak coupling is defined by the Rabi frequency satisfying $\Omega_0/(\omega_x\omega_y\omega_z)^{1/3} = \Omega_0/\bar{\omega} \ll 1$, where $\bar{\omega} = (\omega_x\omega_y\omega_z)^{1/3}$ is the geometric-averaged angular frequency for the trapping potential. By adjusting the laser intensity we can always find the regime in which the spatial and normalized mode functions $\phi_a(\vec{r})$ and $\phi_b(\vec{r})$ vary slowly in time, namely they are “slaved” by the populations [36], so that the parameters k and u also vary slowly in time. Thus in our calculation we can treat the parameters u and k as constants [30,32–34,36,37,51] at least to the zeroth approximation.

3 Entanglement and quantum chaos

3.1 The initial state

To obtain a sharply initial wave packet, we use a generalized spin coherent state (SCS), since it will minimize the initial uncertainty product. Such a state may be defined in the $|j, n\rangle$ basis [53]

$$|\theta, \phi\rangle = \exp[-i\theta(J_x \sin \phi - iJ_y \cos \phi)] |j, -j\rangle. \quad (20)$$

Its properties are given by

$$\begin{aligned} \langle \theta, \phi | \hat{J}_x / j | \theta, \phi \rangle &= \sin \theta \cos \phi, \\ \langle \theta, \phi | \hat{J}_y / j | \theta, \phi \rangle &= \sin \theta \sin \phi, \\ \langle \theta, \phi | \hat{J}_z / j | \theta, \phi \rangle &= -\cos \theta. \end{aligned} \quad (21)$$

In this article, we use the SCS as the initial state so that the mean values of some physical quantities have correspondence in classical phase space.

3.2 Entanglement between the two modes

In previous work, the systems under study are often considered as a collection of N single-qubit subsystems. Bipartite and pairwise entanglement have been used to determine the structure of the entanglement. For instance, in the quantum kicked top, the bipartite entanglement between a pair of qubits and the rest of the system have been calculated to explore the connection between quantum entanglement and chaos. In the coupled kicked top, the bipartite entanglement between the two single kicked tops have been discussed. Since the individual bosons are not physically accessible and distinguishable subsystems of the kicked two-component BEC system, we need to

consider other possible decompositions into subsystems. While we cannot measure which mode a specific particle is in, the occupation number of a given mode is physical observable. In our case, the two modes differ in the internal quantum number, and are a clearly distinguishable subsystem. We can thus regard the two coupled BECs as a bipartite system of the modes. As will be seen later, the entanglement between the two modes has different characteristics compared to the above-mentioned bipartite entanglement. Recently, a scheme of two mode entanglement has been proposed for entanglement swapping in such coupled BEC system.

For pure states, bipartite entanglement is well-defined and can be quantified by the entropy of entanglement of either subsystem. If we initially choose a pure state, the system remains in a pure state at later time. Since we consider only the entanglement of pure states, we will employ the entropy of the subsystem as a measure of the quantum entanglement. More precisely, we will use the von Neumann entropy of the reduced density operator of any subsystem. The reduced density operator of a subsystem is found by tracing out the other subsystem via the partial trace. Once we obtain the reduce density matrix, the entanglement can be readily calculated. If ρ_{ab} is the density operator describing some states of a bipartite system, the reduced density operator for subsystem a is defined by

$$\rho_a = \text{Tr}_b(\rho_{ab}) \quad (22)$$

where Tr_b is the partial trace over subsystem b . The entropy of entanglement is then given by

$$E(\rho_a) = -\text{Tr}(\rho_a \log(\rho_a)) = -\sum_k \lambda_k \log(\lambda_k) \quad (23)$$

where the logarithm is taken in base 2, and $\{\lambda_k\}$ are the set of eigenvalues of the reduced density operator ρ_a . The value of E varies between 0 (for the separable product states) and a maximum of $\log d$ (for the maximally entangled states corresponding to a completely mixed density operator), where d is the dimension of the Hilbert space of the subsystem.

A general state of the system can be expressed in term of the Fock states as

$$|\psi\rangle = \sum_{n=-N/2}^{N/2} c_n(t) |N/2+n\rangle |N/2-n\rangle, \quad (24)$$

which implies that the mode a has $N/2+n$ bosons and the mode b has $N/2-n$ bosons at the same time, where c_n satisfies the normalization condition $\sum_{n=-N/2}^{N/2} |c_n(t)|^2 = 1$.

Using the Fock basis, the density operator is given by

$$\rho_{ab} = |\psi\rangle\langle\psi| = \sum_{n,m=-N/2}^{N/2} c_m c_n^* |m\rangle |N-m\rangle \langle n| \langle N-n|. \quad (25)$$

Here $|m\rangle = |N/2+m\rangle$ has been adopted. The reduced density operator of mode a is obtained by taking the partial

trace with respect to mode b

$$\rho_a = \text{Tr}_b(|\psi\rangle\langle\psi|) = \sum_{n=-N/2}^{N/2} |c_n(t)|^2 |n\rangle\langle n|. \quad (26)$$

From the above expression, we can see that the reduced density operator in the Fock basis is diagonal and the eigenvalues are simply $|c_n(t)|^2$. The entropy of entanglement between the two modes thus reads

$$E(\rho_a) = -\text{Tr}(\rho_a \log \rho_a) = -\sum_{n=-N/2}^{N/2} |c_n(t)|^2 \log |c_n(t)|^2. \quad (27)$$

A simple calculation gives the maximal entanglement

$$E_{max} = -\sum_{n=-N/2}^{N/2} \frac{1}{N+1} \log \frac{1}{N+1} = \log(N+1), \quad (28)$$

which corresponds to a completely mixed density operator.

3.3 The dynamics of entanglement

To begin with, we investigate the dynamics of entanglement for the initial states with the same mean entropy in different regions of the classical phase space. Four areas are of particular interest, namely a fixed point, a stable island, a chaotic sea and the border between the regular and the chaotic regions. We choose the nonlinear parameter $\lambda = 3.5$ for which the phase space is mostly covered by the chaotic region with very clearly regular islands. For convenience, we fix $\theta = 2.32$ and change ϕ to vary through the above-mentioned four different regions, a fixed point occurs at $\phi = 1.19$, a point in the regular region lies at $\phi = 1.40$, a point with $\phi = 2.40$ is inside the chaotic sea and the edge of chaos can be found at $\phi = 1.70$. The initial states are chosen as SCSs with minimum uncertainty and are well localized around the four points in the phase space. In Figure 2, we show the time evolution of the von Neumann entropy. We observe that as the dynamics evolves, the entanglement increases more rapidly for an initial state localized in the chaotic region with $\phi = 2.40$ than ones centered on a fixed point and regular islands. Furthermore, after a short time, the entropy saturates for the initial state inside the chaotic sea. By contrast, the entropy for a fixed point and the stable orbit display a periodic modulation, which is an indicator of the underlying regular classical dynamics. Although the underlying chaos enhance the production of entanglement, we also find that the entanglement between the modes cannot still reach its maximal value E_{max} . The bounds on entanglement due to chaos have been considered within the framework of the random matrix theory [22].

To further display the distinct changes between the regular and chaotic region, we introduce the mean entanglement, which is defined to be averaged over time

$$E_{T'} = \frac{1}{T'} \int_0^{T'} dt E(t). \quad (29)$$

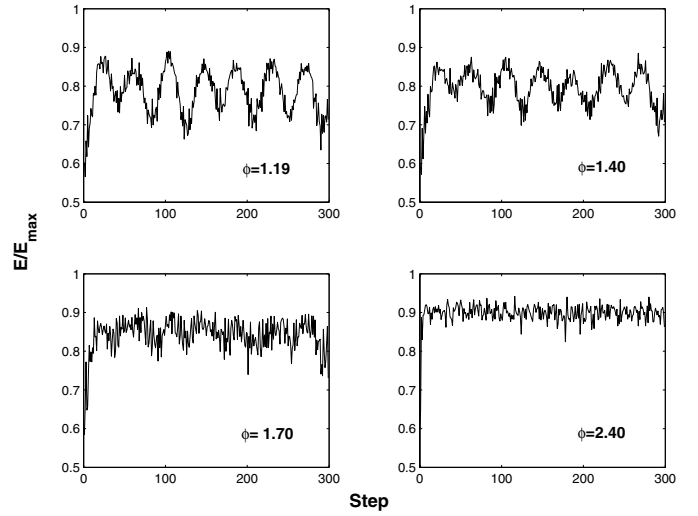


Fig. 2. The dynamical evolution of the von Neumann entropy for different initial SCSs with fixed $\theta = 2.32$. Other parameters are chosen as $\lambda = 3.5$ and $N = 50$.

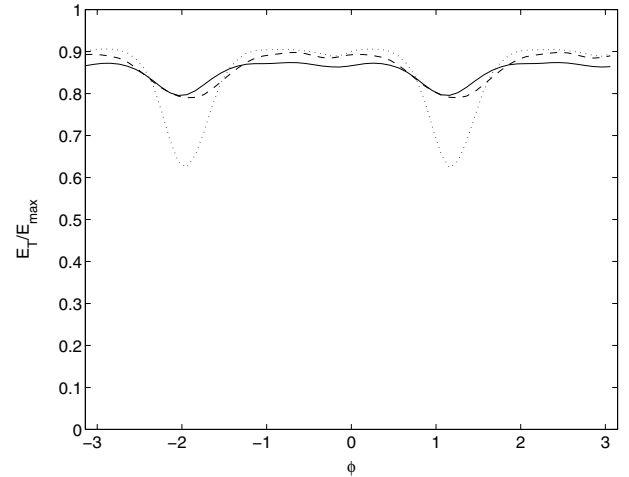


Fig. 3. The mean von Neumann entropy vs the azimuthal angle ϕ . The mean entropy is plotted for $N = 20$ (solid line), $N = 50$ (dashed line) and $N = 100$ (dotted line). Other parameters are the same as in Figure 1. The time average is over 200 steps.

Here the time interval T' should be much longer than the time scale used. We vary the azimuthal angles ϕ from $-\pi$ to π with fixed polar angle θ of the SCS as before. The center of the SCS thus commences inside the chaotic sea and goes through two regular islands. In Figure 3 we display the corresponding numerical results of the mean entanglement E_T . When the azimuthal angles ϕ pass from $-\pi$ to the first regular region, the entropy decreases until it approaches a minimum which corresponds to the fixed point $(\theta, \phi) = (2.32, -1.95)$. Subsequently, the mean entropy increases to a flat larger value corresponding to the chaotic sea. We also observe that as ϕ varies, the mean entropy undergoes two distinct changes at two different increase rates. For example, from the fixed point to the border between the regular and chaotic regions, the mean entropy rises rapidly, and from the border to the chaotic sea, the

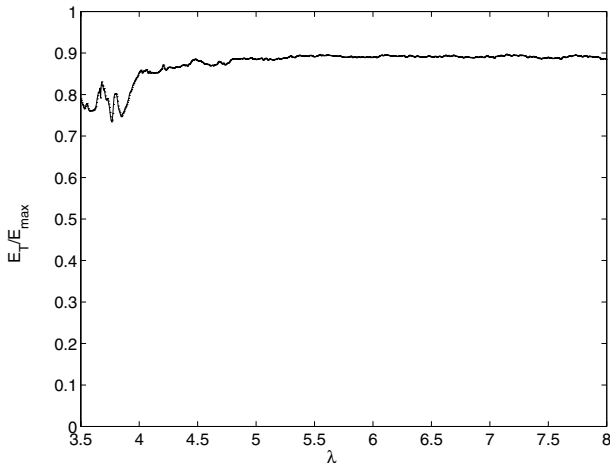


Fig. 4. The mean von Neumann entropy versus the nonlinear parameter λ for the parameter $N = 50$ and the time average over 50 kicks.

mean entropy becomes flat with very tiny change. On the other hand, it is also shown that the larger number of the particle corresponds to the wider regular region. In the larger number limit, the regular region here will coincide with that of classical chaos in Figure 1.

In Figure 4 we show the λ dependence on the mean entropy. When the nonlinear interaction is relative weak, the corresponding classical phase space exhibits clear regular islands inside the chaotic sea, such that the mean entropy displays small oscillations. As the parameter λ rises gradually, the corresponding classical dynamics enters gradually the strong chaos region and the mean entropy displays a rapid increase at $\lambda = 3.80$ and a saturation when $\lambda = 5.00$. Thus, we have a good classical-quantum correspondence.

4 Conclusion

We have examined a kicked two-component BEC system, which obeys collectively the dynamics of the quantum nonlinear top. A more physical description of the system is regarded as a bipartite system, where the subsystems are the two modes. We investigated the relationship between the entanglement of the two modes and the underlying chaos. The classical chaos leads to rapid rise of the entanglement and saturation after a short time. Furthermore, the saturated values of the entanglement fall short of its maximum. The origin of these results lie in the competition between the classical chaos and the quantum phase coherence. In general, chaos tends to lead the system to approach a completely mixed state with the loss of the phase information, in which the von Neumann entropy takes the largest value E_{max} . By contrast, the phase coherence between the two BECs suppresses the increase of entanglement induced by chaos. In the classical limit, the increases in the strength of interaction between atoms drive the system, gradually changing from being mainly regular to being dominantly chaotic. However, the work of Law and coworkers has shown that the relative phase

of the two components can be locked without diffusion when the interaction strength between the two components equals a certain critical value [54].

Recently, quantum computation [55] and quantum information [56] with BEC atoms has been an interesting subject. It is well known that quantum entanglement is a kernel subject in quantum computation and quantum information, thereby, investigating the relation between entanglement and chaos seems to be very important for controlling the quantum entanglement in BECs.

This work was supported by the National Nature Science Foundation of China under Grant No. 10275023.

References

1. S. Lloyd, *Science* **261**, 1589 (1993)
2. C.H. Bennett, S.J. Wiesner, *Phys. Rev. Lett.* **69**, 2881 (1992)
3. C.H. Bennett, G. Brassard, C. Crépeau, R. Jozsa, A. Peres, W.K. Wootters, *Phys. Rev. Lett.* **70**, 1895 (1993)
4. R. Cleve, D. Gottesman, H.-K. Lo, *Phys. Rev. Lett.* **83**, 648 (1999)
5. M.A. Nielsen, I.L. Chuang, *Quantum Computation and Quantum Communication* (Cambridge University Press, Cambridge, 2000)
6. S. Sachdev, *Quantum Phase Transitions* (Cambridge University Press, Cambridge, 1999)
7. A. Osterloh, L. Amico, G. Falci, R. Fazio, *Nature* **416**, 608 (2002)
8. T.J. Osborne, M.A. Nielsen, *Phys. Rev. A* **66**, 032110 (2002)
9. G. Vidal, J.I. Latorre, E. Rico, A. Kitaev, *Phys. Rev. Lett.* **90**, 227902 (2003)
10. N. Lambert, C. Emary, T. Brandes, *Phys. Rev. Lett.* **92**, 073602 (2004)
11. L.F. Santos, G. Rigolin, C.O. Escobar, *Phys. Rev. A* **69**, 042304 (2004)
12. H. Li, X. Wang, B. Hu, e-print [arXiv:quant-ph/0308116](https://arxiv.org/abs/quant-ph/0308116)
13. S. Schneider, G.J. Milburn, *Phys. Rev. A* **65**, 042107 (2002)
14. A.P. Hines, G.J. Milburn, R.H. McKenzie, e-print [arXiv:quant-ph/0308165](https://arxiv.org/abs/quant-ph/0308165)
15. A.P. Hines, C.M. Dawson, R.H. McKenzie, G.J. Milburn, *Phys. Rev. A* **70**, 022303 (2004)
16. F. Haake, *Quantum Signature of Chaos* (Springer, Berlin, 1991)
17. E.J. Heller, *Phys. Rev. Lett.* **53**, 1515 (1984)
18. R. Schack, G.M. D'Ariano, C.M. Caves, *Phys. Rev. E* **50**, 972 (1994)
19. A. Peres, *Phys. Rev. A* **30**, 1610 (1984); J. Emerson, Y.S. Weinstein, S. Lloyd, D.G. Cory, *Phys. Rev. Lett.* **89**, 284102 (2002)
20. K. Furuya, M.C. Nemes, G.Q. Pellegrino, *Phys. Rev. Lett.* **80**, 5524 (1998)
21. R.M. Angelo, K. Furuya, M.C. Nemes, G.Q. Pellegrino, *Phys. Rev. E* **60**, 5407 (1999)
22. P.A. Miller, S. Sarkar, *Phys. Rev. E* **60**, 1542 (1999)
23. J.N. Bandyopadhyay, A. Lakshminarayan, *Phys. Rev. Lett.* **89**, 060402 (2002); J.N. Bandyopadhyay, A. Lakshminarayan, *Phys. Rev. E* **69**, 016201 (2004)

24. H. Fujisaki, T. Miyadera, A. Tanaka, *Phys. Rev. E* **67**, 066201 (2003)
25. X.-W. Hou, B. Hu, *Phys. Rev. A* **69**, 042110 (2004)
26. X. Wang, S. Ghose, B.C. Sanders, B. Hu, *Phys. Rev. E* **70**, 016217 (2004)
27. S. Bettelli, D.L. Shepelyansky, *Phys. Rev. A* **67**, 054303 (2003)
28. T. Prosen, T.H. Seligman, M. Znidaric, *Phys. Rev. A* **67**, 042112 (2003); T. Prosen, T.H. Seligman, *J. Phys. A* **35**, 4707 (2002); S. Schlunk, M.B. d'Arcy, S.A. Gardiner, G.S. Summy, *Phys. Rev. Lett.* **90**, 054101 (2003)
29. C.J. Myatt, E.A. Burt, R.W. Ghrist, E.A. Cornell, C.E. Wieman, *Phys. Rev. Lett.* **78**, 586 (1997); D.S. Hall, M.R. Matthews, J.R. Ensher, C.E. Wieman, E.A. Cornell, *Phys. Rev. Lett.* **81**, 1539 (1998)
30. A.P. Hines, R.H. McKenzie, G.J. Milburn, *Phys. Rev. A* **67**, 013609 (2003)
31. S. Inouye, M.R. Andrews, J. Stenger, H.-J. Miesner, D.M. Stamper-Kurn, W. Ketterle, *Nature* **392**, 151 (1998)
32. A.S. Sørensen, L.-M. Duan, J.I. Cirac, P. Zoller, *Nature* **409**, 63 (2001)
33. L.-M. Kuang, L. Zhou, *Phys. Rev. A* **68**, 043606 (2003)
34. A. Smerzi, S. Fantoni, S. Giovanazzi, S.R. Shenoy, *Phys. Rev. Lett.* **79**, 4950 (1997)
35. G.J. Milburn, J. Corney, E.M. Wright, D.F. Walls, *Phys. Rev. A* **55**, 4318 (1997)
36. J. Williams, R. Walser, J. Cooper, E. Cornell, M. Holland, *Phys. Rev. A* **59**, 31(R) (1999)
37. Y. Wu, X. Yang, *Phys. Rev. A* **68**, 013608 (2003)
38. J. Stenger, S. Inouye, D.M. Stamper-Kurn, H.-J. Miesner, A.P. Chikkatur, W. Ketterle, *Nature* **396**, 345 (1998)
39. F.L. Moore, J.C. Robinson, C.F. Bharucha, B. Sundaram, M.G. Raizen, *Phys. Rev. Lett.* **75**, 4598 (1995)
40. G.J. Milburn, e-print [arXiv:quant-ph/9908037](https://arxiv.org/abs/quant-ph/9908037)
41. G. Gibson, C. Jeffries, *Phys. Rev. A* **29**, 811 (1984); X. Zhang, H. Suhl, *Phys. Rev. A* **32**, 2530 (1985); F.M. de Aguiar, S.M. Rezende, *Phys. Rev. Lett.* **56**, 1070 (1986)
42. K. Nakamura, Y. Okazaki, A.R. Bishop, *Phys. Rev. Lett.* **57**, 5 (1986)
43. G.M. D'Ariano, L.R. Evangelista, M. Saraceno, *Phys. Rev. A* **45**, 3646 (1992)
44. F. Benvenuto, G. Casati, A.S. Pikovsky, D.L. Shepelyansky, *Phys. Rev. A* **44**, 3423(R) (1991); P. Villain, P. Öhberg, M. Lewenstein, *Phys. Rev. A* **63**, 033607 (2001)
45. P. Couillet, N. Vandenberghe, *Phys. Rev. E* **64**, 025202(R) (2001)
46. W. Hai, C. Lee, G. Chong, L. Shi, *Phys. Rev. E* **66**, 026202 (2002); Q. Xie, W. Hai, G. Chong, *Chaos* **13**, 801 (2003); G. Chong, W. Hai, Q. Xie, *Chaos* **14**, 217 (2004); G. Chong, W. Hai, Q. Xie, *Phys. Rev. E* **70**, 036213 (2004); G. Chong, W. Hai, Q. Xie, *Phys. Rev. E* **71**, 016202 (2005)
47. F.Kh. Abdullaev, R.A. Kraenkel, *Phys. Rev. A* **62**, 023613 (2000); R. Franzosi, V. Penna, *Phys. Rev. E* **67**, 046227 (2003)
48. S.A. Gardiner, D. Jaksch, R. Dum, J.I. Cirac, P. Zoller, *Phys. Rev. A* **62**, 023612 (2000); R. Artuso, L. Rebuzzini, *Phys. Rev. E* **66**, 017203 (2002)
49. C. Zhang, J. Liu, M.G. Raizen, Q. Niu, *Phys. Rev. Lett.* **92**, 054101 (2004); G.P. Berman, F. Borgonovi, F.M. Izrailev, A. Smerzi, *Phys. Rev. Lett.* **92**, 030404 (2004)
50. G.J. Duffy, A.S. Mellish, K.J. Challis, A.C. Wilson, *Phys. Rev. A* **70**, 041602(R) (2004); L. Rebuzzini, S. Wimberger, R. Artuso, e-print [arXiv:nlin.CD/0410015](https://arxiv.org/abs/nlin.CD/0410015)
51. C. Menotti, J.R. Anglin, J.I. Cirac, P. Zoller, *Phys. Rev. A* **63**, 023601 (2001); J.R. Anglin, P. Drummond, A. Smerzi, *Phys. Rev. A* **64**, 063605 (2001)
52. D.R. Grempel, R.E. Prange, S. Fishman, *Phys. Rev. A* **29**, 1639 (1984); B.V. Chirikov, *Phys. Rep.* **52**, 263 (1979)
53. F.T. Arecchi, E. Courtens, R. Gilmore, H. Thomas, *Phys. Rev. A* **6**, 2211 (1972)
54. C.K. Law, H. Pu, N.P. Bigelow, J.H. Eberly, *Phys. Rev. A* **58**, 531 (1998)
55. J.K. Pachos, P.L. Knight, *Phys. Rev. Lett.* **91**, 107902 (2003)
56. R. Ionicioiu, P. Zanardi, *Phys. Rev. A* **66**, 050301(R) (2002)